Inverse Field-based Approach for the Evaluation of Electromagnetic Fields and its Application in Local SNR Shimming

Jin Jin[1], Feng Liu[1], Ewald Weber[1], and Stuart Crozier[1]

[1]*The School of Information Technology and Electrical Engineering, The University of Queensland, Brisbane, Queensland, Australia*

INTRODUCTION: A major challenge for high-field magnetic resonance imaging is controlling the transmit radiofrequency (RF) magnetic field (B_1^+) homogeneity and the specific absorption rate (SAR), so that the potential of higher signal-to-noise ratio (SNR) can be realised. The inverse field-based approach was introduced to provide accurate coil receptivity mapping [1-3]. The method was extended in this study to simultaneously estimate, from an experimental image, the transmit and receive radiofrequency (RF) magnetic fields ($\boldsymbol{B_1}^+$and $\boldsymbol{B_1}^-$, bond font indicates complex quantities) and the naturally accompanying electric fields ($\boldsymbol{E_1}$). The resultant signal intensity (SI), $\boldsymbol{B_1}^+$ and $\boldsymbol{B_1}^-$ distributions are tested directly with those acquired from experiments. With the complete knowledge of the electromagnetic fields, a newly developed RF-shimming algorithm more effectively regulated B_1-inhomogeneity, local maximum SAR and local SNR, as compared to traditional methods, namely, phase matching [4], B_1-focusing and power minimization.

METHODOLOGY: The inverse field-based approach for magnetic and electric field mappings can be described as a two-level iterative optimization as follows:

$$\begin{cases} \text{argmin}_{\vec{x}}\left(\min_{M_0,U} \| SI_{CAL} - SI_{EXP} \|_2 \right) & (1a) \\ SI_{CAL} = M_0 |(\boldsymbol{B_1}^-)^*| \sin(V|\boldsymbol{B_1}^+|\gamma\tau) & (1b) \end{cases}$$

where SI_{EXP} denotes intensity image acquired in the experiments (Fig.1b); SI_{CAL} is the signal intensity distribution obtained using Eq.1b, where $\boldsymbol{B_1}^+$ and $\boldsymbol{B_1}^-$ are the circularly polarized components of the transverse magnetic fields obtainable through numerical methods. The inner level of Eq.1 finds the optimal values of sequence-related variables M_0 and U, whereas the outer level searches for the optimal set of geometric variables ($\vec{x}$), so that the difference between SI_{CAL} and SI_{EXP} are minimized.

EXPERIMENTAL VALIDATION: Experiments were performed on a 7T whole body MRI system (Siemens Magnetom) with an in-house built rectangular-shaped transmit/receive surface coil. The coil was loaded with a cylindrical saline phantom of unknown conductivity (σ) and relative permittivity (ε_r). The phantom was placed at the isocentre of the gradient system, whereas the coil was placed a distance (d) away from it on the x-axis (azimuthal angle α=0°). The coil was tuned to 300 MHz for 7T proton applications. An actual flip-angle imaging (AFI) sequence [5] with a 60° nominal flip angle (φ) followed by two delays TR_1 = 20 ms and TR_2 = 300 ms were employed. In the pulsed steady state, two GRE images were acquired at the centre of the phantom as shown in Fig1.a and b, respectively. The φ distribution (Fig.1d) is extracted following the procedure stated in reference [5]. With the imaging results SI_{EXP} and φ known, the relative receptivity (Fig.1g) was estimated ($|\boldsymbol{B_1}^-| = SI_{EXP}/\sin\varphi$). The errors exhibited in φ and $|\boldsymbol{B_1}^-|$ (arrows in Fig.1d and g) stemmed from dividing the intensity image pair, which inevitably produces amplified noise and singularities at the low signal regions. 2D localized polynomial extrapolation was employed to provide corrected estimations (Fig.1e and h).

The optimization process, as described in Eq.1, was implemented in MATLAB (Mathworks, Natick, MA). The optimization exited when stopping criteria were met, arrive at optimal values of d=37.54, σ=0.5118 S/m, ε_r=79.31, α=-1.410°, U=10.92 and M_0=10.00. The resultant SI, flip angle ($\varphi = U|\boldsymbol{B_1}^+|$) and receptivity are shown in Fig1.c, f and i, respectively. The obvious agreement between these field quantities and their experimentally derived counterparts demonstrates the accuracy of the proposed method.

SNR SHIMMING: Utilizing the $\boldsymbol{B_1}^+$, $\boldsymbol{B_1}^-$ and $\boldsymbol{E_1}$ fields derived from the inverse field-based approach, a simple yet effective optimization algorithm was developed to regulate B_1-inhomogeneity, local maximum SAR and local SNR as follows:

$$\text{argmin}_{V_l,\beta_l}\left\{ \sqrt{\frac{\sum_{r\in ROI}\left[\gamma\tau\left|\sum_l V_l e^{-i\beta_l}(\boldsymbol{B_1}^+)_l\right| - FA\right]^2}{N_{ROI}}} + \lambda \frac{\sqrt{\int_{sample}\sigma_r\left|\sum_l(\boldsymbol{E}_r)_l V_l e^{-i\beta_l}\right|^2 dv}}{\left[\sin\left(\gamma\tau\left|\sum_l(\boldsymbol{B_1}^+)_l V_l e^{-i\beta_l}\right|\right)\right]_{SLICE}} \right\} \qquad (2)$$

where $\boldsymbol{E_r}$ and σ_r are the electric field and conductivity at sample location $\boldsymbol{r}$; N_{ROI} is the number of pixels with in the ROI; V_l and β_l are the amplitude and phase of the driving voltage applied on the l^{th} element in the transmission array. The first term of Eq.2 estimates the standard deviation within the RIO of the induced φ with respect the desired flip angle (FA). The second term yields the radio between the noise in the whole subject, which is proportional to the deposited RF energy, and the MR signal from the imaging slice.

The spin density and SNR distributions as a result of employing the traditional RF-shimming algorithms and the SNR shimming methods are shown in Fig.2 and Fig.3, respectively. Comparing to the traditional methods, the SNR-shimming algorithm demonstrated significant improvement on homogenizing spin density, reducing local SAR and enhancing local SNR. Specifically when λ was chosen as $1.95e^{-6}$, with maximum local SAR and B_1-homogeneity better than any of the three traditional algorithms, the proposed method achieved 35% average SNR increase compared to what was achieved using power minimization algorithm.

CONCLUSION: A full-wave field-based approach for electromagnetic field mapping at high fields was presented. The method was validated by 7T saline-phantom imaging studies. This approach facilitated the regulation of B_1-homogeneity, SAR and SNR when a newly developed RF shimming algorithm, dubbed "SNR shimming", was used. In future work, the method will be applied to heterogeneous body models and volunteers to ascertain the advantages in the clinical realm.

[1] J. Jin, et al., 33rd IEEE EMBC, 2011, pp. 2837-2840. [2] J. Jin, et al., ISMRM-ESMRMB 2010, pp. 2896. [3] J. Jin, et al., *J. Magn. Reson.*, vol. 207(1), pp. 59-68, 2010. [4] G.J. Metzger, et al., *Magn. Reson. in Med.*, vol. 59(2), pp. 396-409, 2008. [5] V.L. Yarnykh, *Magnetic Resonance in Medicine*, vol. 57(1), pp. 192-200, 2007.

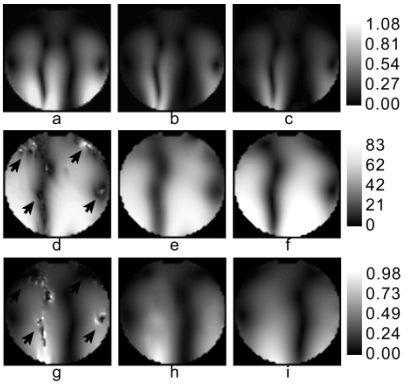

Figure 1 – Experimental validation. (a)-(c) intensity images; (d)-(f): flip angle distributions in degree; (g)-(h): receptivity. First two columns contain experimental results, whereas the last column consists of results from the proposed method. (Read text for more details)

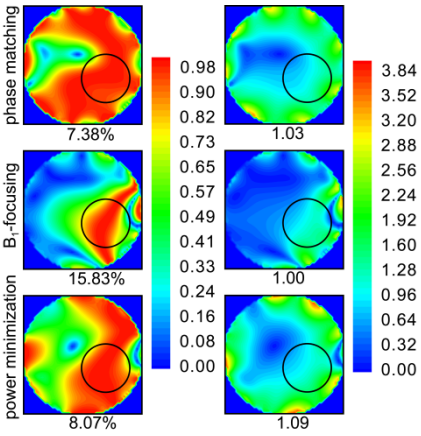

Figure 2 – flip angle (left) and SNR maps (right) of traditional RF-shimming methods. Circles indicate ROIs. Flip angle deviations and relative SNR within the ROIs are indicated by the number below each graph. Maximum SAR averaged over 1cm^3 was 4.23, 10.68 and 5.43 from

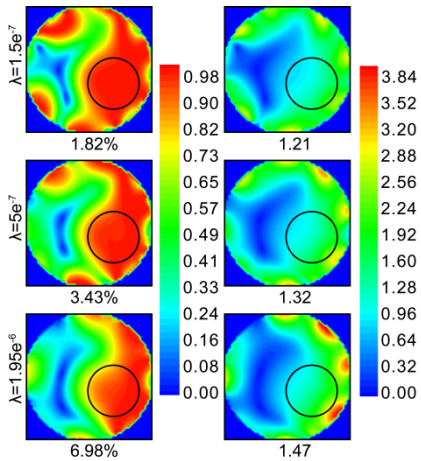

Figure 3 – flip angle (left) and SNR maps (right) of SNR shimming method. ROIs are indicated by the circles. Flip angle deviations and relative SNR within the ROIs are indicated by the number below each graph. Maximum SAR averaged over 1cm^3 was 4.43, 4.12 and 3.33 from top down.